AIAA SciTech Forum
11–15 & 19–21 January 2021, VIRTUAL EVENT
AIAA Scitech 2021 Forum

10.2514/6.2021-1676



# Space-time Galerkin projection via spectral proper orthogonal decomposition and resolvent modes

Aaron Towne*

*Department of Mechanical Engineering, University of Michigan, Ann Arbor MI, USA*



**Most nonlinear reduced-order models are constructed using a set of spatial basis functions (modes) and time dependent expansion coefficients, leading to ordinary differential equations for the expansion coefficients after spatial Galerkin projection of the governing equations. In this paper, we consider instead models based on space-time modes and space-time Galerkin projection for statistically stationary flows. Specifically, we develop a hierarchy of models based on two types of space-time modes – those obtained from spectral proper orthogonal decomposition (SPOD) and resolvent analysis. This leads to a minimization of error over a time window of interest, and the governing equations reduce to a set of algebraic equations for scalar expansion coefficients. The most promising model employs Petrov-Galerkin projection using a trial basis consisting of SPOD modes and a test basis designed to optimally retain the dynamics associated with the leading SPOD modes. We demonstrate the methods using a stochastically forced Ginzburg-landau equation as a simple model for turbulent flows susceptible to high energy amplification, and show that the space-time SPOD Petrov-Galerkin model achieves lower cost and higher accuracy than a standard Galerkin model using proper orthogonal decomposition modes.**

## I. Introduction

Problems in fluid mechanics are typically high dimensional in the sense that they require many degrees of freedom to describe a solution of the discretized equations of motion. As a result, solving the equations can be computationally expensive, especially for turbulent flows. Because of this, reduced order models (ROMs) that can provide accurate approximations of the flow at a lower cost are highly desirable, and the quest to obtain such reduced order models has been an active area of research for many years.[1]

The most common approach to obtain reduced order models of the Navier-Stokes equations is Galerkin projection.[2,3] In this approach, the state vector is written as a summation of orthogonal spatial modes, each weighted by a time-varying expansion coefficient. A coupled set of nonlinear ordinary differential equations (ODEs) for the expansion coefficients is obtained by projecting the governing equations onto the modes. Finally, a reduced order model is obtained by retaining only a subset of the modes, leading to a smaller set of coupled nonlinear ODEs for the remaining expansion coefficients. While in general the modes could correspond to any orthogonal basis, they are most often chosen to be proper orthogonal decomposition (POD) modes.[4] The defining property of POD modes is that they optimally reconstruct the flow energy, computed in a spatial norm and averaged over time, for any order of the expansion. The modes themselves must be computed ahead of time from training data, i.e., a prior simulation of the flow of interest. When POD modes are used as the basis for Galerkin projection, the resulting reduced order model is called a POD Galerkin model.

The energy optimality of POD modes implies neither optimality nor accuracy of the POD Galerkin reduced order model solution. While excellent models can be obtained for some flows,[5] POD Galerkin projection suffers from a number of well-known issues.[3] Errors within the approximation accumulate at every time step, leading to solutions that are often accurate only over short temporal horizons. Indeed, POD Galerkin systems are sometime unstable. Many solutions to these issues have been proposed, most involving the addition of closure terms meant to mimic the dissipitive impact of higher order modes that

*Email for correspondence: towne@umich.edu

have been truncated from the model.[6] Unfortunately, these models tend to be ad hoc and/or tuned to a particular flow, limiting their generalizability. One promising exception is the recent closure strategy based on Mori-Zwanzig formalism.[7] Another well-known approach seeks to stabilize the model by projecting the equations onto a seperate test basis obtained from a least-squares optimization problem.[8]

The limitations of traditional POD Galerkin methods have spurred recent interest in alternative space-time reduced order modeling approaches, including space-time Galerkin projection.[9,10] The essential difference compared to a standard POD Galerkin approach is the use of modes that are functions of both space and time, in contrast to POD modes, which are functions only of space. Expanding the state vector in terms of space-time modes and projecting the equations onto the modes leads to a set of coupled algebratic equations for the expansion coefficients, which are now time-independent scalars. This space-time projection of the equations seeks to minimize error over the full time window for which the modes are defined, providing a means to control the solution error over a desired time window and prevent the error accumulation typical of POD Galerkin methods.

This space-time reduced order modeling framework is currently in its infancy, and there remain many basic questions that have yet to be thoroughly addressed. One of these open questions is the selection of appropriate space-time modes for both the trial basis used to expand the solution and the test basis used to project the governing equations. In this paper, we propose the use of two different types of bases for statistically stationary flows.

The first consists of the modes obtained from spectral proper orthogonal decomposition (SPOD).[11,12] SPOD modes are the solution of a space-time POD optimization problem for stationary flow, and therefore optimally capture the flow energy in a space-time norm.[11,12] In this sense, they are the natural space-time equivalent to standard spatial POD modes. Each SPOD mode oscillates in time at a single frequency, and there exists a complete basis of modes at each frequency. Physically, SPOD modes can be interpreted as coherent structures – portions of the flow that are self-correlated and uncorrelated with all other modes.[12]

The second basis we propose is obtained from resolvent analysis of the Navier-Stokes equations.[13–16] Resolvent analysis identifies frequency-dependent modes that are optimal in terms of their linear gain between the nonlinear and linear fluctuation terms of the Navier-Stokes equations.[16] These modes are obtained via singular value decomposition of the resolvent operator, which constitutes a transfer function between the nonlinear and linear terms in the frequency domain. As in the case of SPOD, this leads to modes that oscillate at a single frequency and form a complete basis at each frequency. Recently, Towne et al.[12] showed that resolvent modes provide an approximation of SPOD modes under the assumption that the nonlinear terms are uncorrelated in space and time, i.e., white noise. While this assumption is never strictly true, resolvent modes have been shown to provide a good approximation of the leading SPOD modes in various turbulent flows.[17,18] The notable advantage of resolvent modes relative to SPOD modes is that their computation does not require training data, apart from a reasonable approximation of the mean flow.

For both the SPOD- and resolvent-based methods we consider both Galerkin methods, for which the same modes are used for the trial and test bases, and Petrov-Galerkin methods, in which the trial and test bases are defined differently. This leads to four distinct models, each with different properties. We will show that a SPOD Petrov Galerkin model, in which the trial basis consists of SPOD modes and the test basis consists of modes that project the equations into a space that optimally governs the leading SPOD modes under certain assumptions, produces the most promising results.

Since both of our proposed bases are made up of single frequency modes, our approach can be understood as a frequency domain reduced order modeling approach. As such, it bears resemblance to the harmonic balance method.[19] The harmonic balance method is a frequency domain approach to solving the Navier-Stokes equations, in which reduction of the model is achieved by truncating low energy frequencies. Our SPOD and resolvent Galerkin and Petrov Galerkin approaches take this one step further by also permitting a reduction of the spatial basis at each frequency. Our SPOD Galerkin approach is also similar in spirit to the SPOD-based reduced order model suggested contemporaneously by Lin;[20] we improve upon their approach by addressing the proper handling of finite time windows and nonlinear terms and by developing a Petrov-Galerkin variant. Our approach differs from the SPOD-based reduced order model of Chu & Schmidt[21] in that we leverage the orthogonal space-time projections enabled by SPOD modes rather than oblique space-only projections as pursued in that work. When using a resolvent basis, our approach is also similar to other efforts to construct nonlinear resolvent models.[22,23]

The remainder of this abstract is arranged as follows. In Section II we review the standard POD Galerkin method and introduce the space-time SPOD Galerkin and resolvent Galerkin methods. Preliminary results obtained from a Ginzburg-Landau model problem are presented in Section III. Ongoing work is discussed in Section IV and the paper is concluded in Section V.

# II. Method

We consider systems of nonlinear ODEs of the form

$$\frac{d\boldsymbol{q}}{dt} - A\boldsymbol{q} = \boldsymbol{n}(\boldsymbol{q}) + B\boldsymbol{\eta}, \tag{1}$$

where the vector $\boldsymbol{q}(t) \in \mathbb{C}^N$ represents the state of the spatially discretized equations, i.e., every flow variable at every grid point in the domain. The Navier-Stokes equations can be naturally cast in the form of (1) by applying a Reynolds decomposition, in which case $\boldsymbol{q}$ represents the fluctuation to the mean, $A \in \mathbb{C}^{N\times N}$ is the linearized Navier-Stokes operator, $\boldsymbol{n}(\boldsymbol{q}) \in \mathbb{C}^N$ contains the remaining nonlinear fluctuation terms, and $\boldsymbol{\eta}(t) \in \mathbb{C}^{N'}$ represents external excitations, which are mapped onto the equations of motion by the operator $B \in \mathbb{C}^{N\times N'}$. Writing the governing equations in the form of (1) with the linear and nonlinear terms explicitly separated[24] will allow us to use concepts from resolvent analysis and SPOD to design an approach that optimally preserves the linear amplification mechanisms within the flow. We wish to obtain reduced forms of equation (1) involving $r < N$ unknowns.

## II.A. POD Galerkin and Petrov-Galerkin projection

Before introducing the new space-time approaches, we briefly review the standard Galerkin projection and Petrov-Galerkoin projection methods. Using a set of orthogonal modes $\{\boldsymbol{\phi}_k : k = 1, \ldots, N\}$ called the trial basis, the state vector $\boldsymbol{q}$ can be expanded as

$$\boldsymbol{q}(t) = \sum_{k=1}^{N} \boldsymbol{\phi}_k a_k(t) = \Phi\boldsymbol{a}(t), \tag{2}$$

where the $k$-th column of the matrix $\Phi$ is $\boldsymbol{\phi}_k$ and the $k$-th entry of the vector $\boldsymbol{a}$ is $a_k$. We also define a second orthogonal basis $\{\boldsymbol{\psi}_k : k = 1, \ldots, N\}$ called the test basis, which can be compactly expressed by the matrix $\Psi$ whose $k$-th column is $\boldsymbol{\psi}_k$. Each set of modes in orthogonal in the inner product

$$\langle \boldsymbol{u}, \boldsymbol{v} \rangle_x = \boldsymbol{v}^* W \boldsymbol{u}, \tag{3}$$

where $W$ is a positive-definite weight matrix. The orthogonality of the modes is expressed as, e.g., $\langle \boldsymbol{\phi}_i, \boldsymbol{\phi}_k \rangle_x = \boldsymbol{\phi}_i^* W \boldsymbol{\phi}_k = \delta_{ik}$, with equivalent expressions for the test basis.

A coupled set of ODEs governing $\boldsymbol{a}$ can be obtained by inserting the expansion (2) into (1) and projecting the equation onto $\Psi$, i.e, left-multiplying the equations by $\Psi^* W$. Applying the preceding steps leads to $N$ coupled ODEs for $\boldsymbol{a}$,

$$\Psi^* W \Phi \frac{d\boldsymbol{a}}{dt} - \Psi^* W A \Phi \boldsymbol{a} = \Psi^* W \left[\boldsymbol{n}(\Phi\boldsymbol{a}) + B\boldsymbol{\eta}(t)\right]. \tag{4}$$

A reduced order system can be obtained by truncating the expansion of $\boldsymbol{q}$ to its leading $r$ terms, i.e.,

$$\boldsymbol{q}(t) \approx \sum_{j=1}^{r} \boldsymbol{\phi}_j a_j(t) = \Phi_r \boldsymbol{a}_r(t), \tag{5}$$

where $\Phi_r$ and $\boldsymbol{a}_r$ contain the first $r$ column of $\Phi$ and $r$ elements of $\boldsymbol{a}$, respectively. Likewise, the test basis is truncated to its leading $r$ modes, which are contained in $\Psi_r$. Then, (4) becomes

$$\Psi_r^* W \Phi_r \frac{d\boldsymbol{a}_r}{dt} - \Psi_r^* W A \Phi_r \boldsymbol{a}_r = \Psi_r^* W \left[\boldsymbol{n}(\Phi_r\boldsymbol{a}_r) + B\boldsymbol{\eta}(t)\right]. \tag{6}$$

This is an approximate evolution equation for $\boldsymbol{a}_r$, since the impact of higher modes has been neglected.

This approach is called Galerkin projection when the trial and test bases are the same, i.e., $\Psi_r = \Phi_r$. When the basis is specified as POD modes, this approach is called the POD Galerkin method. If distinct trial and test bases are employed, the approach is called Petrov-Galerkin projection, variants of which using POD modes for the trial basis have been developed.[8]

### II.B. Space-time Galerkin and Petrov-Galerkin projection in the frequency domain

This time, consider space-time trial and test bases of the form $\{\boldsymbol{\phi}_{jk} e^{\mathrm{i}\omega_j t} : j = 1, \ldots, N_\omega; k = 1, \ldots, N\}$ and $\{\boldsymbol{\psi}_{jk} e^{\mathrm{i}\omega_j t} : j = 1, \ldots, N_\omega; k = 1, \ldots, N\}$, respectively. Here, $j$ selects the frequency $\omega_j$ of the mode, $k$ indicates the mode number at a particular frequency, and $N_\omega$ is the total number of frequencies included in the expansion. In practice, the total number of frequencies, and their specific values, are determined by the number and spacing of the discrete time instances that are included within the optimization window. The modes in each basis are orthogonal in a space-time inner product

$$\langle \boldsymbol{u}, \boldsymbol{v} \rangle_{x,t} = \int_{-\infty}^{\infty} \boldsymbol{v}^*(t) W \boldsymbol{u}(t) dt = \int_{-\infty}^{\infty} \langle \boldsymbol{u}, \boldsymbol{v} \rangle_x \, dt. \tag{7}$$

Using this trial basis, the state vector can be expanded as

$$\boldsymbol{q}(t) = \sum_{j=1}^{N_\omega} \sum_{k=1}^{N} \boldsymbol{\phi}_{jk} a_{jk} e^{\mathrm{i}\omega_j t} = \sum_{j=1}^{N_\omega} \Phi_j \boldsymbol{a}_j e^{\mathrm{i}\omega_j t}, \tag{8}$$

where the $k$-th column of the matrix $\Phi_j$ is $\boldsymbol{\phi}_{jk}$ and the $k$-th entry of the vector $\boldsymbol{a}_j$ is $a_{jk}$. Inserting (8) into (1) leads to

$$\sum_{j=1}^{N_\omega} (\mathrm{i}\omega_j - A) \Phi_j \boldsymbol{a}_j e^{\mathrm{i}\omega_j t} = \boldsymbol{f}(t), \tag{9}$$

where we have introduced the function

$$\boldsymbol{f}(t) = \boldsymbol{n}(\boldsymbol{q}(t)) + B\boldsymbol{\eta}(t) + \boldsymbol{f}_0(t) = \boldsymbol{n}\left( \sum_{j=1}^{N_\omega} \Phi_j \boldsymbol{a}_j e^{\mathrm{i}\omega_j t} \right) + B\boldsymbol{\eta}(t) + \boldsymbol{f}_0(t) \tag{10}$$

to simplify the notation in what follows. The term $\boldsymbol{f}_0$ has been added to lift the initial condition at $t = 0$ to the forcing such that it need not be further considered. It is important to keep in mind that $\boldsymbol{f}$ is a nonlinear function of the complete set of expansion coefficients $\boldsymbol{a}$, where $\boldsymbol{a}$ is the union of $\boldsymbol{a}_j$ for all $j$.

Next, we project (9) onto the set of modes $\Psi_l$ at frequency $\omega_l$ by left-multiplying by $e^{-\mathrm{i}\omega_l t} \Psi_l^* W$ and integrating over all times,

$$\int_{-\infty}^{\infty} \sum_{j=1}^{N_\omega} \Psi_l^* W (\mathrm{i}\omega_j - A) \Phi_j \boldsymbol{a}_j e^{\mathrm{i}\omega_j t} e^{-\mathrm{i}\omega_l t} dt = \int_{-\infty}^{\infty} \Psi_l^* W \boldsymbol{f}(t) e^{-\mathrm{i}\omega_l t} dt. \tag{11}$$

After some algebra, this can be written as

$$\left( \sum_{j=1}^{N_\omega} \Psi_l^* W (\mathrm{i}\omega_j - A) \Phi_j \boldsymbol{a}_j \right) \left[ \int_{-\infty}^{\infty} e^{\mathrm{i}\omega_j t} e^{-\mathrm{i}\omega_l t} dt \right] = \Psi_l^* W \left[ \int_{-\infty}^{\infty} \boldsymbol{f}(t) e^{-\mathrm{i}\omega_l t} dt \right]. \tag{12}$$

The term in square brackets on the left–hand-side integrates to a Dirac delta function; we replace this with a Kronecker delta $\delta_{jl}$ in recognition that the integral will ultimately be taken over a finite interval. The term in square brackets on the right-hand-side integrates to $\hat{\boldsymbol{f}}(\omega_l)$, the Fourier transform of $\boldsymbol{f}$ evaluated at frequency $\omega_l$. Making these substitutions and applying the delta function leaves

$$(\mathrm{i}\omega_l \Gamma_l - A_l) \, \boldsymbol{a}_l = B_l \hat{\boldsymbol{f}}(\omega_l) \tag{13}$$

for $l = 1, \ldots, N_\omega$, with $\Gamma_l = \Psi_l^* W \Phi_l \in \mathbb{C}^{N \times N}$, $A_l = \Psi_l^* W A \Phi_l \in \mathbb{C}^{N \times N}$, and $B_l = \Psi_l^* W \in \mathbb{C}^{N \times N}$.

A reduced-order expression can be obtained by replacing $\Phi_l$ and $\Psi_l$ with their truncated forms $\Phi_{l,r}$ and $\Psi_{l,r}$ consisting of their first $r$ columns and, if desired, by reducing the number of retained frequencies, yielding

$$(\mathrm{i}\omega_l \Gamma_{l,r} - A_{l,r}) \, \boldsymbol{a}_{l,r} = B_{l,r} \hat{\boldsymbol{f}}(\omega_l) \tag{14}$$

with

$$\Gamma_{l,r} = \Psi_{l,r}^{*} W \Phi_{l,r} \in \mathbb{C}^{r\times r}, \tag{15}$$

$$A_{l,r} = \Psi_{l,r}^{*} W A \Phi_{l,r} \in \mathbb{C}^{r\times r}, \tag{16}$$

$$B_{l,r} = \Psi_{l,r}^{*} W \in \mathbb{C}^{r\times N}, \tag{17}$$

and $\boldsymbol{a}_{l,r} \in \mathbb{C}^{r}$.

In the case where the ODE in (1) is nonlinear, i.e., $\boldsymbol{n} \neq \boldsymbol{0}$, the right-hand-side of (13) is a function of the expansion coefficients for all retained frequencies. Thus, (13) must be solved simultaneously for all $N_\omega^{'}$ retained frequencies, giving an $rN_\omega^{'}$ dimensional system of nonlinear algebraic equations to be solved for the complete set of expansion coefficients $\boldsymbol{a}$. In the case where the original ODE is linear, $\hat{\boldsymbol{f}}$ is not a function of $\boldsymbol{a}$, so (13) gives a decoupled $r$-dimensional linear system to be solved individually for each $\boldsymbol{a}_l$.

In the following sections, we consider several different choices for the trial and test bases. If the trial and test bases are selected to be the same, this will lead to a frequency domain space-time Galerkin ROM; if they are chosen to be different, we obtain a frequency-domain space-time Petrov-Galerkin ROM.

### II.C. SPOD Galerkin projection

SPOD modes are obtained from a space-time POD problem under the condition of statistically stationary flow. Specifically, in terms of our semi-discrete formulation (discretized in space) we seek time-varying modes $\phi(t)$ that maximize the expected value of the energy

$$\lambda = \frac{E\{|\langle \boldsymbol{q}(t), \boldsymbol{\phi}(t)\rangle_{x,t}|^2\}}{\langle \boldsymbol{\phi}(t), \boldsymbol{\phi}(t)\rangle_{x,t}}, \tag{18}$$

where the expectation is an ensemble average over realizations of the flow and the space-time inner product in defined in (7).

The modes that maximize (18) are solutions of the space-time eigenvalue problem

$$\int_{-\infty}^{\infty} C(t,t') W \boldsymbol{\phi}(t') dt' = \lambda \boldsymbol{\phi}(t), \tag{19}$$

where $C(t,t')$ is the two-point space-time correlation tensor of the data. For statistically stationary data, $C(t,t') \to C(t-t')$ and the solutions of (19) take the form

$$\boldsymbol{\phi}(t) = \boldsymbol{\phi}_{ij} e^{\mathrm{i}\omega_j t}, \tag{20}$$

where each $\boldsymbol{\phi}_{ij}$ satisfies the frequency-domain eigenvalue problem

$$S_{qq}(\omega_j) W \boldsymbol{\phi}_{ij} = \lambda_{ij} \boldsymbol{\phi}_{ij} \tag{21}$$

and $S_{qq}(\omega)$ is the cross-spectral density (CSD) tensor, i.e., the Fourier transform of $C(t-t')$ or, equivalently,

$$S_{qq} = E\{\hat{\boldsymbol{q}}\hat{\boldsymbol{q}}^{*}\}. \tag{22}$$

At each frequency, there exists a complete basis of modes that are orthogonal in the spatial inner product (3). The complete set of modes over all frequencies are orthogonal in the space-time inner product (7). The eigenvalues $\lambda_{ij}$ indicate the contribution of each mode to the total energy of the flow.

To summarize, SPOD modes provide an optimal, orthogonal space-time basis for capturing the energy of statistically stationary flows. The form of the complete set of SPOD modes described above is the same as that assumed in Section II.B. Thus, a space-time SPOD Galerkin projection ROM in the form of in (14) - (17) is obtained by selecting the trial and tests bases, $\Psi_l$ and $\Phi_l$, respectively, to be SPOD modes. Using the spatial SPOD orthogonality condition, $\Psi_j^{*} W \Psi_j = I$, leads to the simplification $\Gamma_{l,r} = I_r$. The resulting ROM is the natural space-time analogue of the standard POD Galerkin approach.

### II.D. Resolvent Galerkin projection

One disadvantage of both POD and SPOD Galerkin approaches is that time-resolved training data in the form of a prior simulation (or experiment) of the flow are required to compute the bases. In this section, we propose a variation of the SPOD Galerkin approach that requires only an estimate of the mean flow to compute the space-time basis.

The approach is based on resolvent analysis of the governing equations.[13–16] Taking a Fourier transform of (1) leads to an expression of the form

$$L\hat{\boldsymbol{q}} = \hat{\boldsymbol{f}}, \tag{23}$$

where

$$L(\omega) = (\mathrm{i}\omega I - A)\,. \tag{24}$$

Solving for $\hat{\boldsymbol{q}}$ gives

$$\hat{\boldsymbol{q}} = R\hat{\boldsymbol{f}}, \tag{25}$$

where

$$R(\omega) = (\mathrm{i}\omega I - A)^{-1} \tag{26}$$

is termed the resolvent operator. Orthogonal modes that optimally represent the energy gain

$$\sigma^2 = \frac{\langle \hat{\boldsymbol{q}}, \hat{\boldsymbol{q}} \rangle_x}{\langle \hat{\boldsymbol{f}}, \hat{\boldsymbol{f}} \rangle_x} \tag{27}$$

can be obtained by computing the singular value decomposition

$$W^{1/2} R W^{-1/2} = \tilde{U}\Sigma\tilde{V}^* \tag{28}$$

and defining $U = W^{-1/2}\tilde{U}$ and $V = W^{-1/2}\tilde{V}$.[12] The columns of $U$ and $V$ provide orthogonal sets of modes, called output and input modes, respectively, in the inner product (3) for each frequency, and the square-root of the gain of each mode is given by the associated singular value, found on the diagonal of $\Sigma$. The resolvent operator can be recovered as

$$R = U\Sigma V^* W. \tag{29}$$

The resolvent output modes $U$ share the same space-time orthogonality as SPOD modes and the leading $r$ modes can be used for the trial and test bases $\Phi_j$ and $\Psi_j$ to obtain a resolvent Galerkin projection ROM. Again, the orthogonality of the resolvent output modes leads to the simplification $\Gamma_{l,r} = I_r$.

### II.E. Resolvent Petrov-Galerkin projection

Resolvent analysis is often understood in terms of the linear input-output behavior of the governing equations. Specifically, a truncation of the resolvent operator in terms of its singular modes optimally preserves the input-output behavior of the linearized equations. The resolvent Galerkin approach developed in the previous section does not take advantage of this property of resolvent modes or the underlying input-output perspective on the governing equations.

In this section, we seek trial and test bases that lead to a Petrov-Galerkin projection that optimally preserves the input-output behavior of the linear part of (1). Using the result from Towne et al.[12] that resolvent modes optimally capture the flow energy (i.e., are equivalent to SPOD modes) when the nonlinear forcing forcing terms are spatially uncorrelated (white), this objective can be equivalently stated as seeking bases that minimize the error of the Petrov-Galerkin ROM under the approximation that the forcing is white. This white-noise assumption has been employed in numerous previous models based on the linearized Navier-Stokes equations in general and resolvent analysis in particular.

To make this white-noise-forcing assumption explicit, we rewrite (23) and (25) as

$$L\hat{\boldsymbol{q}} = \hat{\boldsymbol{w}} \tag{30}$$

and

$$\hat{\boldsymbol{q}} = R\hat{\boldsymbol{w}}, \tag{31}$$

respectively, where $\hat{\boldsymbol{w}}$ is spatially uncorrelated at every frequency, i.e., $E\{\hat{\boldsymbol{w}}\hat{\boldsymbol{w}}^*\} = c_f(\omega)I$. Without loss of generality, we take the frequency dependent amplitude to be $c_f(\omega) = 1$.

The optimal rank-$r$ approximation of $\hat{\boldsymbol{q}}$ is

$$\hat{\boldsymbol{q}} \approx U_r \Sigma_r V_r^* W \hat{\boldsymbol{w}}, \tag{32}$$

where $\Sigma_r$ contains the leading $r$ singular values. This optimal approximation was obtained by first solving the linear system (30) to obtain (31) and then reducing the rank of $R$. Thus, it does not constitute a ROM in the sense defined in this paper, since it required solution of the full-order system. In what follows, we will show that this optimal rank-$r$ solution (32) can be achieved via Petrov-Galerkin projection of (30) using trial and test bases corresponding to output and input resolvent modes, respectively.

While intuitive, this result is not already implied by (32); the solve-then-reduce approach used to obtain (32) need not produce the same approximation as the reduce-then-solve approach described below that is needed to obtain a ROM. Indeed, these two approximation are only equivalent for this problem when the trial and test bases are are chosen to be the same as the bases used to reduce the rank of $R$ in the solve-then-reduce case. Thus, the reduce-then-solve ROM produces the optimal solution only when the trial and test bases are chosen to be output and input resolvent modes, respectively.

To show that the proposed resolvent Petrov-Galerkin ROM recovers the optimal solution in (32), we begin by writing $L$ in (30) in term of resolvent modes,

$$V \Sigma^{-1} U^* W \hat{\boldsymbol{q}} = \hat{\boldsymbol{w}}. \tag{33}$$

Using the leading $r$ resolvent output modes as a trial basis,

$$\hat{\boldsymbol{q}} \approx U_r \boldsymbol{a}, \tag{34}$$

and the leading $r$ resolvent input modes as the test basis gives

$$V_r^* W V \Sigma^{-1} U^* W U_r \boldsymbol{a} = V_r^* W \hat{\boldsymbol{w}} \tag{35}$$

upon substitution of (34) and projection of (33) against the test basis. Due to the orthogonality of $U_r$ and $V_r$ in a $W$-weighted inner product, (35) reduces to

$$\Sigma_r^{-1} \boldsymbol{a} = V_r^* W \hat{\boldsymbol{w}}. \tag{36}$$

Solving (36) for $\boldsymbol{a}$ and substituting the solution back into (34) recovers the optimal solution (32). Therefore, Petrov-Galerkin projection using resolvent output and input modes as the trial and test bases, respectively, minimizes the error of the ROM under the assumption that the nonlinear terms from the governing equations are white. Or equivalently stated, it optimally preserves the linear input-output behavior of the equations.

### II.F. SPOD Petrov-Galerkin projection

The previous section showed that resolvent output and input modes constitute optimal trial and test bases, respectively, for space-time Petrov-Galerkin projection of stationary flows under the asusmption that the nonlinear fluctuation terms from Navier-Stokes are white. However, a large number of studies in recent years[12, 25] have shown that the nonlinear terms in real flows are not white and that accounting for their color is critical for obtaining accurate models. In this section, we show how optimal trial and test bases can be obtained by accounting for the color of the nonlinear forcing terms, which is quantified by the forcing CSD

$$S_{ff} = E\{\hat{\boldsymbol{f}} \hat{\boldsymbol{f}}^*\}. \tag{37}$$

Our approach is to manipulate (23) into the form of (30), for which we already know the optimal trial and test bases from the previous section. This can be accomplished by whitening the forcing. The first step is to decompose the forcing CSD (37) as

$$S_{ff} = F F^*, \tag{38}$$

which can be obtained using a Cholesky of SPOD (eigenvalue) decomposition, among other choices. Then, left-multiplying (23) by $F^{-1}$ gives

$$F^{-1} L \hat{\boldsymbol{q}} = F^{-1} \hat{\boldsymbol{f}} = \hat{\boldsymbol{w}}. \tag{39}$$

To see that the final equality holds, i.e., that the modified forcing $F^{-1}\hat{\boldsymbol{f}}$ is white, notice that

$$E\left\{\left(F^{-1}\hat{\boldsymbol{f}}\right)\left(F^{-1}\hat{\boldsymbol{f}}\right)^*\right\} = F^{-1} S_{ff} \left(F^*\right)^{-1} = I. \tag{40}$$

Solving (39) for $\hat{\boldsymbol{q}}$ gives

$$\hat{\boldsymbol{q}} = R_F \hat{\boldsymbol{w}}, \tag{41}$$

where

$$R_F = RF = U_F \Sigma_F V_F W. \tag{42}$$

From Section II.E, we know that the optimal truncation of (42) is given by the resolvent modes and singular values of $R_F$ (denoted $U_F$, $\Sigma_F$, and $V_F$) and the optimal trial and test bases for Petrov-Galerkin projection are the output and input resolvent modes of $R_F$, respectively. Thus, the optimal ROM is obtained by substituting the expression

$$\hat{\boldsymbol{q}} \approx U_{F,r} \boldsymbol{a} \tag{43}$$

into (39) and projecting onto the test basis $V_{F,r}$, i.e.,

$$V_{F,r}^* W F^{-1} L U_{F,r} \boldsymbol{a} = V_{F,r}^* W F^{-1} \hat{\boldsymbol{f}}. \tag{44}$$

Solving (44) for $\boldsymbol{a}$ for all frequencies (recall that $\hat{\boldsymbol{f}}$ is a nonlinear function of $\boldsymbol{a}$ if the system is nonlinear) and substituting the result into (43) gives the optimal solution under the assumption that the nonlinear term can be treated as a colored external forcing of the linear dynamics. If the system is linear, $\hat{\boldsymbol{f}}$ is not a function of $\boldsymbol{a}$ and solving (44) for $\boldsymbol{a}$ and combining with (43) gives

$$\hat{\boldsymbol{q}} \approx U_{F,r} \left( V_{F,r}^* W F^{-1} L U_{F,r} \right)^{-1} V_{F,r}^* W F^{-1} \hat{\boldsymbol{f}}. \tag{45}$$

As shown above, the optimal trial basis is given by the output modes of $R_F$. Towne et al.[26] showed that these modes correspond exactly to the SPOD modes of the flow. This result is significant in that it confirms that we are using the optimal basis for capturing the flow energy of the fully nonlinear system even though we used a linear input-output perspective in which the nonlinearity is treated in a statistical sense to determine the optimal the bases.

The test basis, given by the input modes of $R_F$, are also closely related to SPOD modes. Beginning with the second equality in (42), using that $R = L^{-1}$ by definition, and solving for $V_F$ gives

$$V_F = F^{-1} L U_F \Sigma_F. \tag{46}$$

We know that $U_F$ contains SPOD modes and $\Sigma_F$ contains the square roots of the SPOD eigenvalues. By comparing (46), (23), and (40), we see that the test basis consists of whitened forces associated with the SPOD modes. Thus, the test basis $V_{F,r}$ projects the governing equations into a space in which the impact of the nonlinear forcing on the leading SPOD modes is optimally retained. Inspecting (45), we see that the test basis that should be applied to the original, un-whitened equation (23) is

$$\Psi_{j,r} = W^{-1} (F^{-1})^* W V_{F,r}. \tag{47}$$

From (47) and (46), we can see that, given knowledge of the SPOD modes, we can obtain the test basis without the need to form the modified resolvent operator $R_F$ or compute resolvent modes of any kind. Because the trial basis consists of SPOD modes and the test basis can be constructed from the same SPOD modes, we call this approach SPOD Petrov-Galerkin projection.

# III. Results

In this section, the methods described above are demonstrated using the linearized complex Ginzburg-Landau equation, which has been used by several previous authors[12,27–30] as a convenient one-dimensional model that mimics key properties of the linearized Navier-Stokes operator for real flows. Application to more complicated nonlinear ODEs is currently underway.

## III.A. The complex Ginzburg-Landau equation

The linearized Ginzburg-Landau operator takes the form

$$\mathcal{A} = -\nu \frac{\partial}{\partial x} + \gamma \frac{\partial^2}{\partial x^2} + \mu(x), \tag{48}$$

which after discretization in $x$ yields the operator $A$ in (1). Several variants of the function $\mu(x)$ have been used in the literature; here the quadratic form

$$\mu(x) = (\mu_0 - c_\mu^2) + \frac{\mu_2}{2}x^2 \tag{49}$$

is adopted.[27–29] All of the parameters in (48) and (49) are set to the values used previously by Towne *et al.*[12] With these parameters, the leading singular value of $R$ at its peak frequency is ten times larger than the second singular value, which is a typical value for real flows. Following Bagheri *et al.*,[28] the equations are discretized with a pseudo-spectral approach using $N = 220$ Hermite polynomials.

The discretized equations are stochastically excited in the time domain using forcing terms with prescribed statistics identical to those used by Towne *et al.*[12] In particular, the forcing is spatially correlated and qualitatively similar to the nonlinear terms in real flows, such as a turbulent jet.[26] The equations are integrated using a fourth-order embedded Runge-Kutta method,[31] and a total of 30000 snapshots of the solution are collected with spacing $\Delta t = 0.5$, leading to a Nyquist frequency of $\omega_{Nyquist} = 2\pi$. Two-thirds of these snapshots are used to compute modes and the remaining one-third is used to test the models. The test data are organized into an ensemble of blocks containing $N_\omega = 2048$ snapshots; each block represents a different realization of the stochastic system, enabling computation of solution and error statistics averaged over the ensemble. Each block is windowed using a sixth-order sine window[32] to avoid signal processing issues; proper handling of windows is discussed in Section IV.



### III.B. Reduced order model results

In this section, we will compare results obtained from each of the reduced order models described in Section II. Several options exist for making comparisons between the different models: we could hold constant either the order, cost, or accuracy of the models, and the other two would then vary. As a starting point, we fix the order of the approximation, i.e., the total number of space-time degrees of freedom available to each model to describe the solution over the interval of interest. For the standard POD-Galerkin model, this is equal to the number of modes in the expansion times the number of time instances within the interval. For the frequency domain models, it is equal to the number of frequencies (which is also nominally equal to the number of discrete time instances within the interval) times the number of modes retained in the expansion *at each frequency.* In what follows, we consider $r = 10$ modes over intervals containing $N_\omega = 2048$ frequencies (and time instances), as mentioned previously.

Since each model requires different computations, they will have different costs despite each model containing the same total number of degrees of freedom. For the above choices, the costs of the full-order Ginzburg-Landau equations, POD Galerkin, SPOD Galerkin, resolvent Galerkin, resolvent Petrov-Galerkin, and SPOD Petrov-Galerkin models, measured in wall-time on a single processor, are 276, 57, 0.29, 0.30, and 0.41 seconds, respectively. It is clear that, at least for the linear test case considered here, the frequency-domain models are able to provide a representation of the solution with a fixed number of degrees of freedom at much lower cost compared to a standard time-domain POD-Galerkin model. In the following sections, we will examine several metrics of solution accuracy of each method.

#### *III.B.1. Comparisons in the time domain*

Figure 1 shows an example of the time-domain solution obtained from the full-order ODE (blue solid line), POD Galerkin model (black dotted line), SPOD Galerkin model (orange dashed line), resolvent Galerkin mode (purple dashed line), resolvent Petrov-Galerkin mode (maroon dashed line), and SPOD Petrov-Galerkin model (green dashed line). Figure 1(a) shows the real part of the solution at $x = 5$ for one realization of the system. All five models provide a reasonable approximation of the full-order solution, but the SPOD Petrov-Galerkin model in particular appears to lead to the lowest errors. This is confirmed in Figure 1(b), which shows the real part of the difference between each ROM solution and the full-order solution for the same realization. The squared magnitude of the error averaged over the ensemble of realizations is shown in Figure 1(c). All four frequency-domain models lead to lower error than the standard POD Galerkin model. Both resolvent-based methods yield very similar results. This will be repeatedly observed in the following sections and is likely due to the similarity of the input and output resolvent modes for the Ginzburg-Landau system. The error for SPOD Galerkin model is higher than the other frequency-domain models, but still lower than the standard POD Galerkin model. As expected, the SPOD Petrov-Galerkin model produces the lowest error, around an order of magnitude lower than the POD Galerkin model.

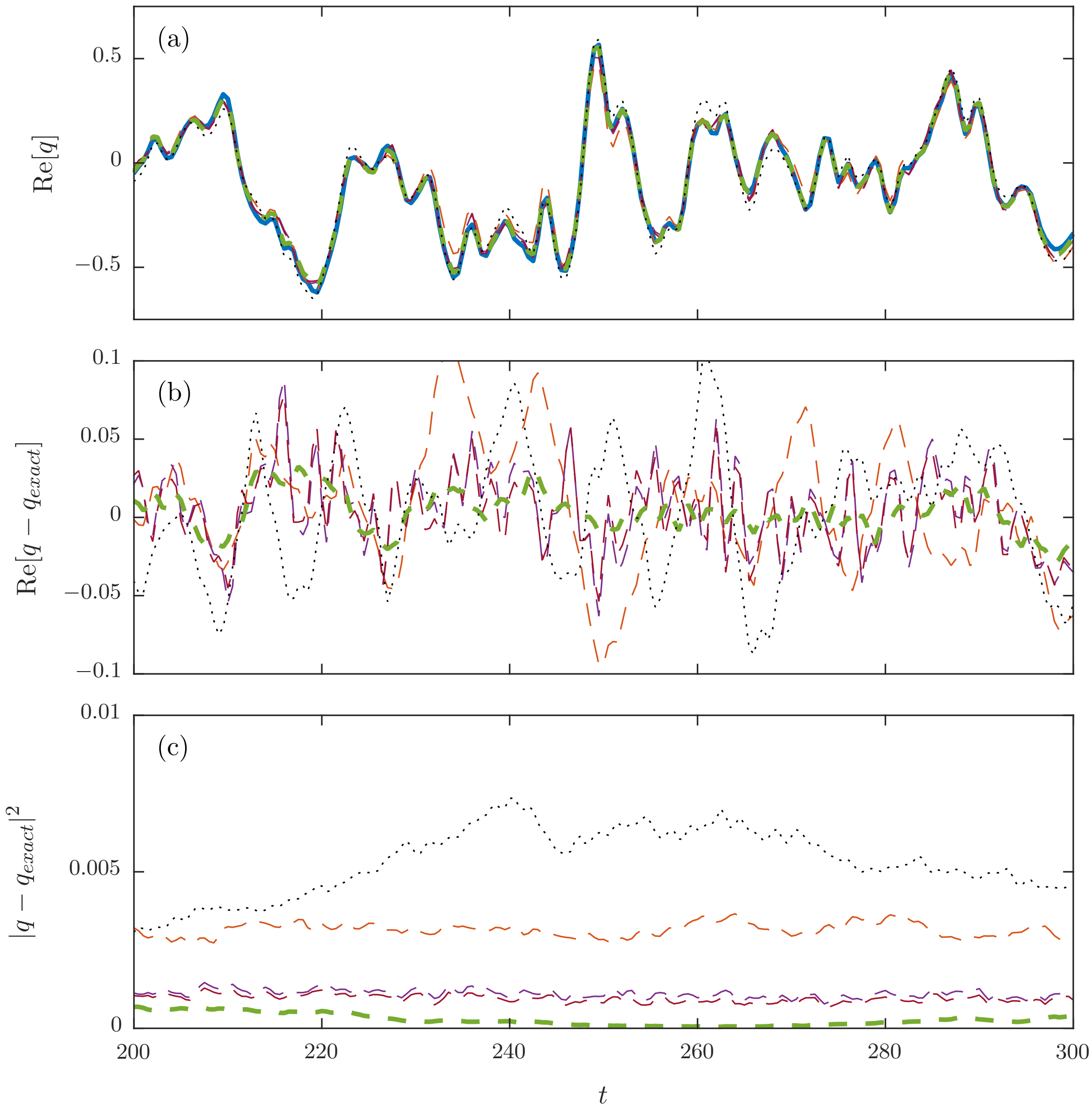


Figure 1: Time-domain solution at $x = 5$: (a) real part of one realization of the system; (b) real part of the error in the same realization; (c) squared amplitude of the error averaged over all realizations of the system. Legend: full-order ODE (blue solid line), POD Galerkin model (black dotted line), SPOD Galerkin model (orange dashed line), resolvent Galerkin mode (purple dashed line), resolvent Petrov-Galerkin mode (maroon dashed line), and SPOD Petrov-Galerkin model (green dashed line).

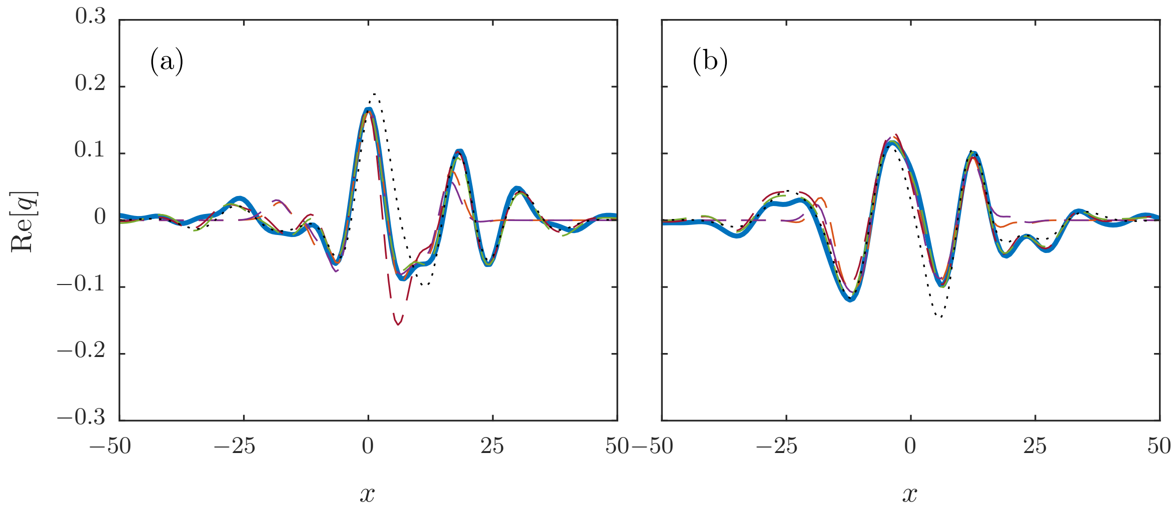


Figure 2: Real part of the solution as a function of $x$ at two time instances for a single realization of the system: (a) $t = 260$; (b) $t = 300$. Legend: full-order ODE (blue solid line), POD Galerkin model (black dotted line), SPOD Galerkin model (orange dashed line), resolvent Galerkin mode (purple dashed line), resolvent Petrov-Galerkin mode (maroon dashed line), and SPOD Petrov-Galerkin model (green dashed line).

Figure 2 shows the real part of the full-order and ROM solutions at two instances in time, $t = 260$ and 300, as a function of $x$ for the same realization of the system considered in Figure 1. Additionally, Figure 3 shows the squared amplitude of the error averaged over the ensemble of realizations as a function of $x$. The SPOD Petrov-Galerkin model provides the most accurate solution over most of the $x$ domain, consistent with the results observed at $x = 5$. The POD Galerkin and SPOD Galerkin models achieve similar error levels except near their peak value, but the latter does so with two orders of magnitude lower cost. The two resolvent-based ROMs have a lower peak error but struggle for larger $|x|$ values. This can be explained by the fact that the leading resolvent modes have concentrated support at low $|x|$ values and are nearly zero at larger $|x|$ values; they therefore have limited ability to represent the data for larger $|x|$ values that is excited by the colored forcing. This can be seen clearly in Figure 2; both resolvent-based ROMs yield solutions that are nearly zero for $|x| > 20$, in contrast to the data. This highlights the importance of accounting for the colored statistics of the forcing in defining appropriate modes. The forcing color is implicitly included in the POD and SPOD Galerkin models (the data used to compute the modes includes the influence of the forcing color) and explicitly in the SPOD Petrov-Galerkin model.

*III.B.2. Comparisons in the frequency domain*

Next, we compares the various ROM solutions in the frequency domain to further elucidate their properties. The four frequency-domain models are naturally represented in the frequency domain, and frequency-domain representations of the full-order and POD Galerkin models are obtained using a discrete Fourier transform over the interval defining each realization of the system. Figure 4 shows an example of the Fourier modes of one realization of the solution obtained from each method as a function of $x$ at four different frequencies, $\omega = -1.5$, $-0.6$, $-0.2$, and 1. Again, the SPOD Petrov-Galerkin solution is noticeably better than the other models.

More quantitative comparisons can be made by computing the error between the full-order and reduced-order solutions averaged over the ensemble of realizations of the system. Figure 5 shows the power spectral density of the error for (a) the POD Galerkin, (b) resolvent Galerkin, (c) resolvent Petrov-Galerkin, (d) SPOD Galerkin, and (e) SPOD Petrov-Galerkin models as a function of $\omega$ and $x$. Panel (f) shows results from a full-order frequency-domain model to be discussed later. The contour levels span four orders of magnitude with the largest value set to the maximum error in the SPOD Petrov-Galerkin results. All of the

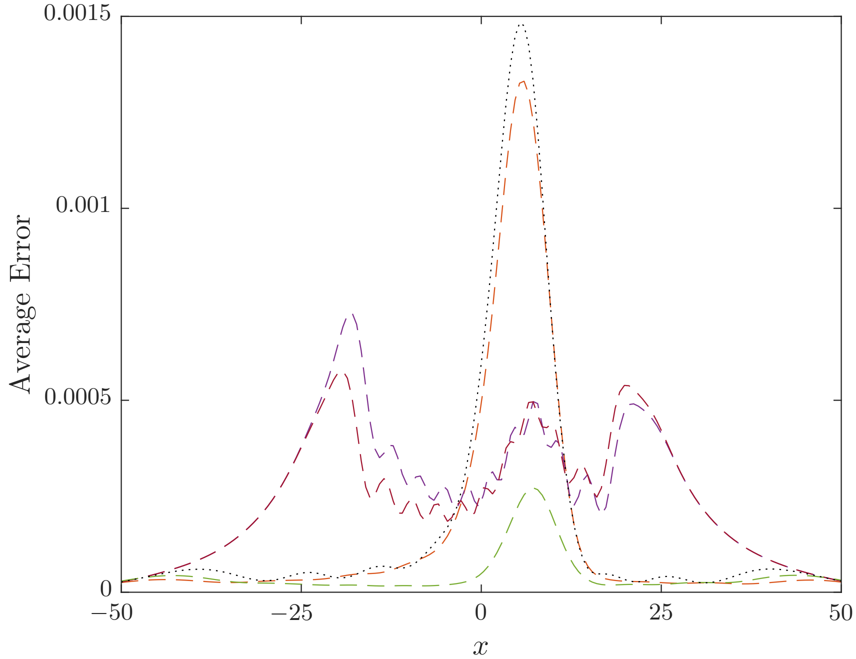


Figure 3: Squared amplitude of the error as a function of $x$ averaged over the ensemble of realization. Legend: full-order ODE (blue solid line), POD Galerkin model (black dotted line), SPOD Galerkin model (orange dashed line), resolvent Galerkin mode (purple dashed line), resolvent Petrov-Galerkin mode (maroon dashed line), and SPOD Petrov-Galerkin model (green dashed line).

models exhibit a peak in error at low $\omega$ and $x$ values, which also corresponds to the region where the solution is most energetic. The POD and SPOD Galerkin results are again very similar. The two resolvent-based models have lower peak errors but much higher errors away from the peak. A similar observation was made in Figure 3, but here we see that the inability of the resolvent models to represent the data at large $|x|$ values persists at all frequencies. Finally, the SPOD Petrov-Galerkin model yields the lowest error virtually everywhere in the $\omega$ - $x$ plane.

Figure 6 shows the total mean error measured in the norm induced by the $W$-weighted inner product as a function of $\omega$, providing a global measure of the error as a function of frequency. The error of the SPOD Petrov-Galerkin model (green dashed line) is consistently lower than the POD Galerkin model (black solid line) and the other frequency-domain models.

## IV. Ongoing work: accounting for finite windows

While these preliminary results are promising, there are a number of additional important issues that must be addressed to realize the potential of the frequency-domain space-time ROMs developed in this paper. Critically, the impact of the use of a finite temporal window must be accounted for in the derivation of the method.[32] In practice, the infinite integrals in (12) must be approximated over a window $[0, T]$ of finite length $T$. This practical restriction can be incorporated into the derivation by using a modified form of (12),

$$\left(\sum_{j=1}^{N_\omega} \Psi_l^* W(\mathrm{i}\omega_j - A)\Psi_j \boldsymbol{a}_j\right)\left[\int_{-\infty}^{\infty} w(t)e^{\mathrm{i}\omega_j t}e^{-\mathrm{i}\omega_l t}dt\right] = \Psi_l^* W\left[\int_{-\infty}^{\infty} \boldsymbol{f}(t)w(t)e^{-\mathrm{i}\omega_l t}dt\right], \tag{50}$$

where $w(t)$ is a window function that is zero outside of the interval $[0, T]$. Evaluating the integrals then leads to a modified form of (13),

$$\sum_{j=1}^{N_\omega} \Psi_l^* W(\mathrm{i}\omega_j - A)\Psi_j \boldsymbol{a}_j \hat{w}(\omega_j - \omega_l) = B_l \hat{\boldsymbol{f}}_w(\omega_l), \tag{51}$$

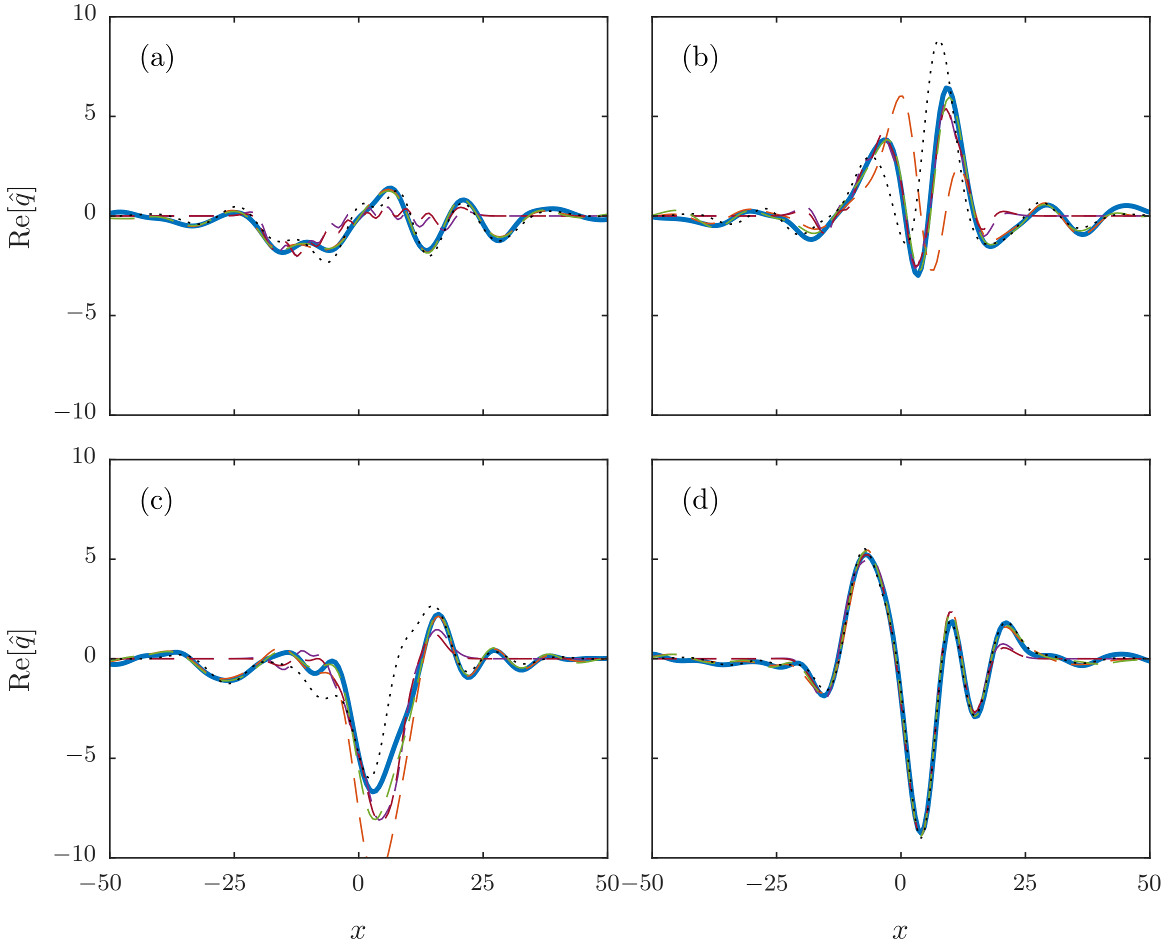


Figure 4: Real part of the solution as a function of $x$ for fixed frequencies: (a) $\omega = -1.5$; (b) $\omega = -0.6$; (c) $\omega = -0.2$; (d) $\omega = 1$. Legend: full-order ODE (blue solid line), POD Galerkin model (black dotted line), SPOD Galerkin model (orange dashed line), resolvent Galerkin mode (purple dashed line), resolvent Petrov-Galerkin mode (maroon dashed line), and SPOD Petrov-Galerkin model (green dashed line).

where $\hat{\boldsymbol{f}}_w$ is the windowed Fourier transform of $\boldsymbol{f}$ and $\hat{w}$ is the Fourier transform of the window function.

As $T \to \infty$, $\hat{w}(\omega_j - \omega_l)$ necessarily approaches the the delta function $\delta_{jl}$ (recall that wide functions in the time domain become narrow functions in the frequency domain), thus recovering the infinite time solution in (13). However, for finite $T$, the $\hat{w}(\omega_j - \omega_l)$ term couples together all frequencies on the left-hand-side of (51), in contrast to (13). For nonlinear systems, different frequencies were already coupled through the dependence of $\hat{\boldsymbol{f}}_l$ on the complete set of expansion coefficients. However, $\hat{w}(\omega_j - \omega_l)$ leads to coupled equations even for linear systems.

This finite-time-horizon induced linear coupling was not accounted for in the Ginzburg-Landau results reported in Section III, and the impact of neglecting this effect can be observed by considering the results shown in Figure 5(f). Here, we show the error obtained using a full-order frequency-domain model, i.e., we solve (9) with a complete basis at every frequency. Since we have not truncated the basis in this case, the error should, in theory, be zero if the time interval were infinite. By necessity, a finite interval was used (a total of $N_\omega = 2048$ time steps), leading to the observed error. It is notable that at low frequencies and $|x|$ values the SPOD Petrov-Galerkin model (with $r = 10$ modes) achieves almost the same error as the full-order mode; this indicates that the errors observed in the SPOD Petrov-Galerkin model in this region are not primarily due to the reduction of the model order, but to the neglect of the linear coupling terms created by the use of a finite time window. This provides hope that still lower errors can be achieved by

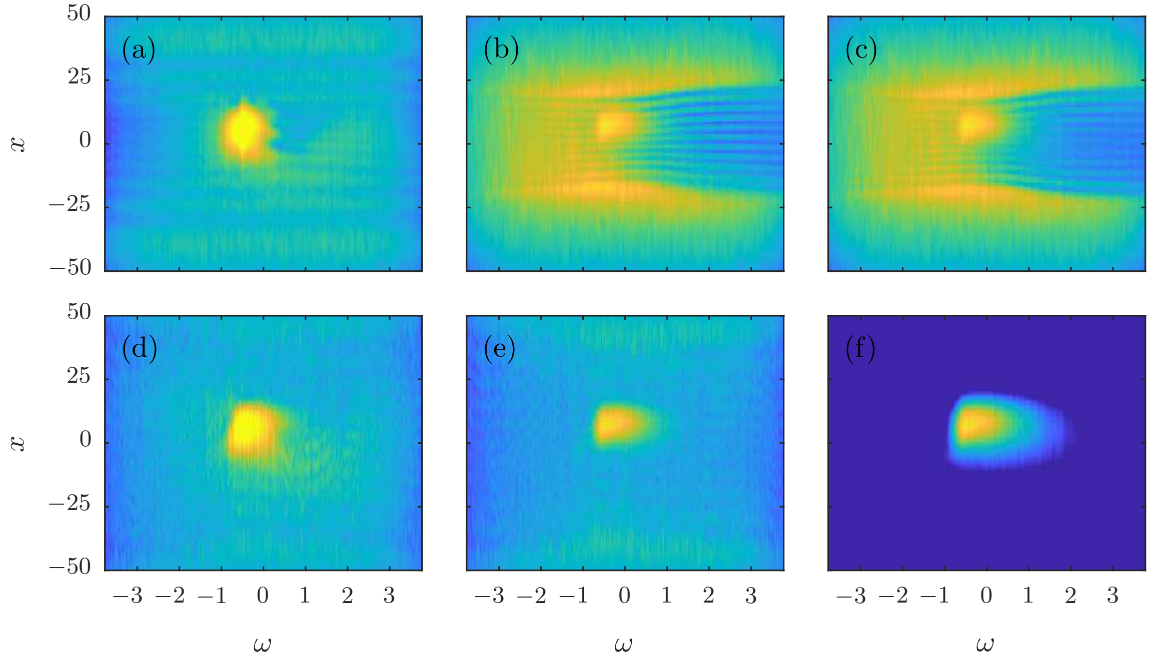


Figure 5: Mean-squared error as a function of $\omega$ and $x$: (a) POD Galerkin model; (b) resolvent Galerkin mode; (c) resolvent Petrov-Galerkin mode; (d) SPOD Galerkin model; (e) SPOD Petrov-Galerkin model; (f) full-order frequency-domain model.



properly accounting for windowing effects.

## V. Conclusions

In summary, we have developed a suite of new reduced order models based on space-time Galerkin projection using SPOD and resolvent modes. The approach has the potential to overcome issues commonly encountered when using traditional POD Galerkin models, such as error accumulation and instability as the ODEs governing the time-dependent expansion coefficients are advanced in time. In contrast, the space-time methods minimize errors over a desired time interval, leading to algebraic equations for time-independent expansion coefficients.

Several variants of the space-time models were derived using a resolvent-analysis-inspired input-output perspective on the governing equations, culminating in a SPOD Petrov-Galerkin model that optimally accounts for the color of the nonlinear and/or external forcing terms. The trial basis consists of SPOD modes, which provide an optimal basis for the solution even for nonlinear systems, and a separate test basis projects the governing equations into a space in which the impact of the forcing terms on the leading SPOD modes is optimally retained on average.

The reduced cost and improved accuracy of the space-time models over a standard POD Galerkin model was demonstrated for a linear Ginzburg-Landau equation. For a fixed number of space-time degrees of freedom, all of the frequency-domain models were around two orders of magnitude faster than the POD Galerkin model. The SPOD Petrov-Galerkin model produced errors that were consistently an order of magnitude lower than the POD Galerkin model in several different metrics. Additional improvements are expected by accounting for the use of finite time windows. The success of the new models for this linear test problem by no means guarantees success for nonlinear problems, and we are currently in the process of testing our methods for several nonlinear problems.

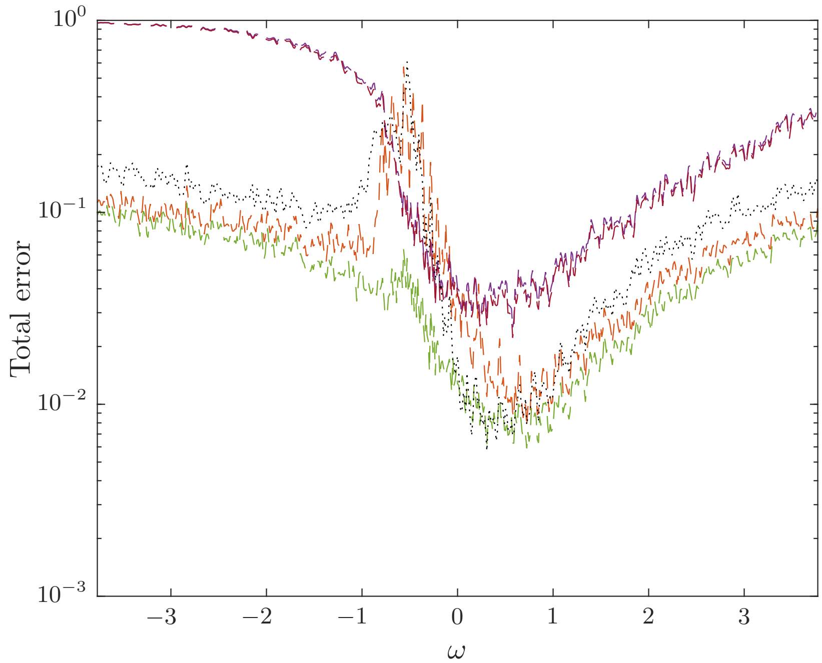


Figure 6: Power spectral density of the total solution error integrated over the domain as a function of $\omega$. Legend: full-order ODE (blue solid line), POD Galerkin model (black dotted line), SPOD Galerkin model (orange dashed line), resolvent Galerkin mode (purple dashed line), resolvent Petrov-Galerkin mode (maroon dashed line), and SPOD Petrov-Galerkin model (green dashed line).

## References


[1] Holmes, P., Lumley, J. L., Berkooz, G., and Rowley, C. W., *Turbulence, Coherent Structures, Dynamical Systems and Symmetry*, Cambridge Monographs on Mechanics, Cambridge University Press, 2nd ed., 2012.

[2] Noack, B. R., Afanasiev, K., Morzynski, M., Tadmor, G., and Thiele, F., "A hierarchy of low-dimensional models for the transient and post-transient cylinder wake," *J. Fluid Mech.*, Vol. 497, 2003, pp. 335–363.

[3] Rowley, C. W. and Dawson, S. T. M., "Model reduction for flow analysis and control," *Annu. Rev. Fluid Mech.*, Vol. 49, 2017, pp. 387–417.

[4] Sirovich, L., "Turbulence and the dynamics of coherent structures. I. Coherent structures," *Quart. Appl. Math.*, Vol. 45, No. 3, 1987, pp. 561–571.

[5] Rowley, C. W., Colonius, T., and Murray, R. M., "Model reduction for compressible flows using POD and Galerkin projection," *Physica D*, Vol. 189, No. 1, 2004, pp. 115–129.

[6] Östh, J., Noack, B. R., Krajnović, S., Barros, D., and Borée, J., "On the need for a nonlinear subscale turbulence term in POD models as exemplified for a high-Reynolds-number flow over an Ahmed body," *J. Fluid Mech.*, Vol. 747, 2014, pp. 518–544.

[7] Parish, E. J., Wentland, C., and Duraisamy, K., "The Adjoint Petrov-Galerkin Method for Non-Linear Model Reduction," *arXiv:1810.03455*, 2018.

[8] Carlberg, K., Bou-Mosleh, C., and Farhat, C., "Efficient non-linear model reduction via a least-squares Petrov–Galerkin projection and compressive tensor approximations," *Int. J. Numer. Meth. Eng.*, Vol. 86, No. 2, 2011, pp. 155–181.

[9] Choi, Y. and Carlberg, K., "Space–Time Least-Squares Petrov–Galerkin Projection for Nonlinear Model Reduction," *SIAM Journal on Scientific Computing*, Vol. 41, No. 1, 2019, pp. A26–A58.

[10] Parish, E. J. and Carlberg, K. T., "Windowed least-squares model reduction for dynamical systems," *arXiv:1910.11388*, 2019.

[11] Lumley, J. L., *Stochastic tools in turbulence*, Academic Press, New York, 1970.

[12] Towne, A., Schmidt, O. T., and Colonius, T., "Spectral proper orthogonal decomposition and its relationship to dynamic mode decomposition and resolvent analysis," *J. Fluid Mech.*, Vol. 847, 2018, pp. 821–867.

[13] Trefethen, L., Trefethen, A., Reddy, S., and Driscoll, T., "Hydrodynamic stability without eigenvalues," *Science*, Vol. 261, No. 5121, 1993, pp. 578–584.

[14] Jovanović, M. R. and Bamieh, B., "Componentwise energy amplification in channel flows," *Journal of Fluid Mechanics*, Vol. 534, 2005, pp. 145–183.

[15] Sipp, D., Marquet, O., Meliga, P., and Barbagallo, A., "Dynamics and control of global instabilities in open-flows: a linearized approach," *Appl. Mech. Rev.*, Vol. 63, No. 3, 2010.

[16]McKeon, B. J. and Sharma, A. S., "A critical-layer framework for turbulent pipe flow," *J. Fluid Mech.*, Vol. 658, 2010, pp. 336–382.

[17]Schmidt, O. T., Towne, A., Rigas, G., Colonius, T., and Brès, G. A., "Spectral analysis of jet turbulence," *J. Fluid Mech.*, Vol. 855, 2018, pp. 953–982.

[18]Symon, S., Sipp, D., and McKeon, B. J., "A tale of two airfoils: resolvent-based modelling of an oscillator versus an amplifier from an experimental mean," *J. Fluid Mech.*, Vol. 881, 2019, pp. 51–83.

[19]Hall, K. C., Thomas, J. P., and Clark, W. S., "Computation of unsteady nonlinear flows in cascades using a harmonic balance technique," *AIAA J.*, Vol. 40, No. 5, 2002, pp. 879–886.

[20]Lin, C., *Model order reduction in the frequency domain via spectral proper orthogonal decomposition*, Ph.D. thesis, University of Illinois at Urbana-Champaign, 2019.

[21]Chu, T. and Schmidt, O. T., "Towards reduced-order SPOD-Galerkin models for turbulent flows," *Bulletin of the American Physical Society*, 2019.

[22]Rosenberg, K. and McKeon, B. J., "Efficient representation of exact coherent states of the Navier–Stokes equations using resolvent analysis," *Fluid Dyn. Research*, Vol. 51, No. 1, 2019, pp. 011401.

[23]Rigas, G., Sipp, D., and Colonius, T., "Nonlinear input-output analysis of laminar-turbulent transition for wall-bounded flows," *Bulletin of the American Physical Society*, 2019.

[24]Sipp, D., de Pando, M. F., and Schmid, P. J., "Nonlinear model reduction: a comparison between POD-Galerkin and POD-DEIM methods," *arXiv preprint arXiv:2005.03173*, 2020.

[25]Zare, A., Jovanović, M. R., and Georgiou, T. T., "Colour of turbulence," *J. Fluid Mech.*, Vol. 812, 2017, pp. 636–680.

[26]Towne, A., Brès, G. A., and Lele, S. K., "A statistical jet-noise model based on the resolvent framework," *AIAA Paper #2017-3406*, 2017.

[27]Hunt, R. E. and Crighton, D. G., "Instability of flows in spatially developing media," *Proc. R. Soc. London Ser. A*, Vol. 435, The Royal Society, 1991, pp. 109–128.

[28]Bagheri, S., Henningson, D. S., Hoepffner, J., and Schmid, P. J., "Input-output analysis and control design applied to a linear model of spatially developing flows," *Appl. Mech. Rev.*, Vol. 62, No. 2, 2009, pp. 020803.

[29]Chen, K. K. and Rowley, C. W., "$H_2$ optimal actuator and sensor placement in the linearised complex Ginzburg–Landau system," *J. Fluid Mech.*, Vol. 681, 2011, pp. 241–260.

[30]Towne, A., Lozano-Durán, A., and Yang, X., "Resolvent-based estimation of space-time flow statistics," *J. Fluid Mech.*, Vol. 883, 2020, pp. A17.

[31]Shampine, L. F. and Reichelt, M. W., "The Matlab ODE suite," *SIAM J. Sci. Comput.*, Vol. 18, No. 1, 1997, pp. 1–22.

[32]Martini, E., Cavalieri, A. V. G., Jordan, P., and Lesshafft, L., "Accurate Frequency Domain Identification of ODEs with Arbitrary Signals," *arXiv:1907.04787*, 2019.